Evidence of interlamellar failure in environmental stress cracking of polyethylene.

The environmental stress cracking (ESC) of polyethylene is brittle in nature, although the material otherwise fails by cold drawing and necking. From scanning electron microscope observation, Hannon [1] proposed that the failure, almost totally brittle microscopically, was caused by nucleation and growth of holes followed by viscoelastic deformation of the molecules surrounding them.

We are investigating the fundamental mechanism of the ESC phenomenon, i.e. precisely what effect the environment brings about in the material so that it fails in a brittle manner, instead of failing in its usual ductile way. Our scanning electron microscopic studies have revealed some very interesting features which show the basic role of the environment in the ESC phenomenon. Consequently, although the study is continuing and details will be published at a later date, it appears worthwhile to report some of these findings.

The ESC tests reported here have been carried out on a series of low density polyethylenes (LDPE) having melt flow indices (MFI) of 0.25, 2.5 and 20. The material was compression-moulded into sheets which were quenched to room temperature from 180° C and subsequently annealed at 100° C for 3 h. Double edge-notched specimens containing sharp razor-blade cuts at the notch tips were cut from the sheets and tested under dead weight loading at low stresses in 10% Igepal Co–630 detergent at 25° C. The fracture surfaces were sputter coated with gold and then observed in a Cambridge scanning electron microscope. In all the figures the crack propagates from left to right.

To compare the mechanism of ESC failure with that in air, a few tests were done in air on similar LDPE specimens under dead weight load. The environmentally cracked specimens showed no appreciable sign of the thickness contraction or plastic deformation which was present in the specimens which failed in air.

At low magnifications in the ESC specimens, the crack surface appears to consist of fibrils, and the extent of fibrillation, i.e. the surface roughness, was more for the lower MFI materials. These fibrils may either be favourably oriented in the material or become oriented upon application of the load. The surface of the air-tested specimen, on the contrary, shows material flow in the direction of crack propagation, excepting just at the crack tip; Figs. 1 and 2 show two such surfaces.

The most interesting features are observed at higher magnifications. Figs. 3 and 4 were taken at similar locations to Figs. 1 and 2 respectively, but at higher magnifications. Fig. 3 shows the evidence of interlamellar failure, whereas Fig. 4 still shows that failure in air is mainly due to cold drawing and necking. Fig. 5 elaborates the interlamellar failure of a fibril in Fig. 3. It should be noted at

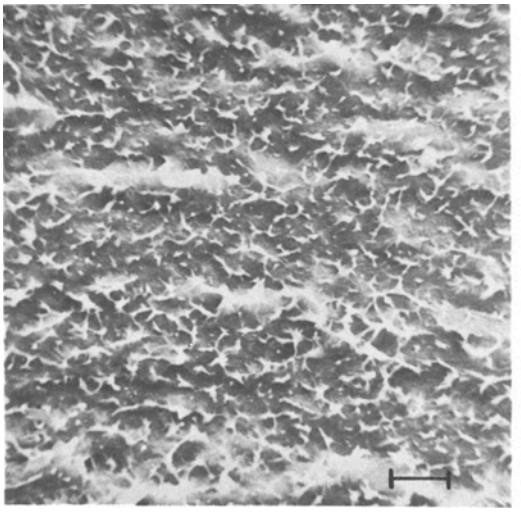

Figure 1 ESC fracture surface of LDPE, MFI 2.5 (Scale 20 μm).

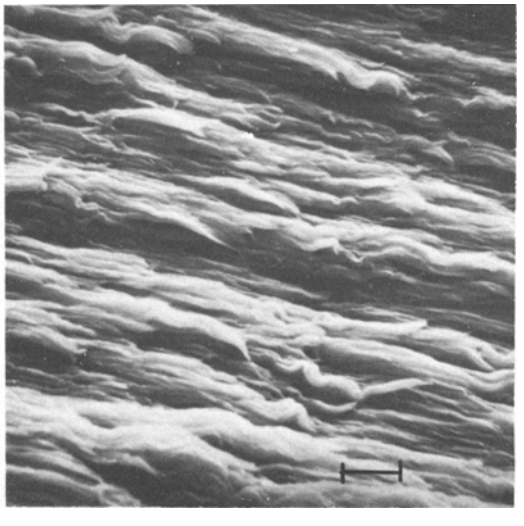

Figure 2 Fracture surface of LDPE failed in air, MFI 20 (Scale 10 μm).

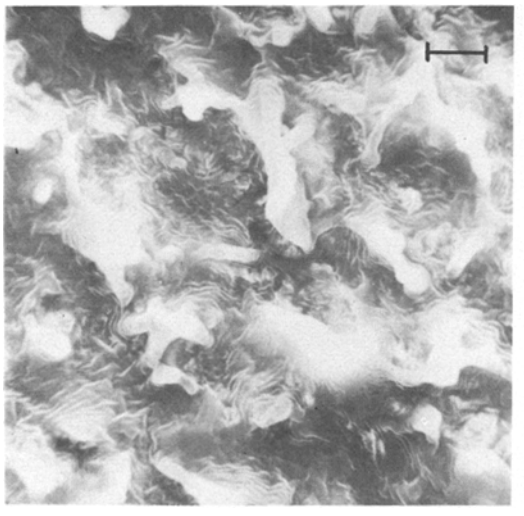

Figure 3 Higher magnification of central portion of Fig. 1 (Scale 5 μm).

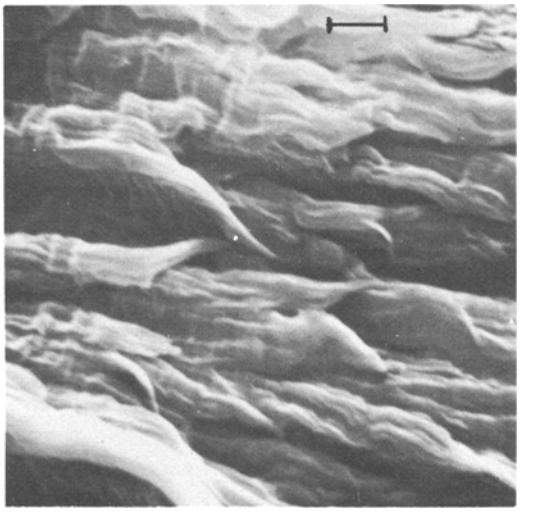

Figure 4 Higher magnification of Fig. 2 (Scale 2 μm).

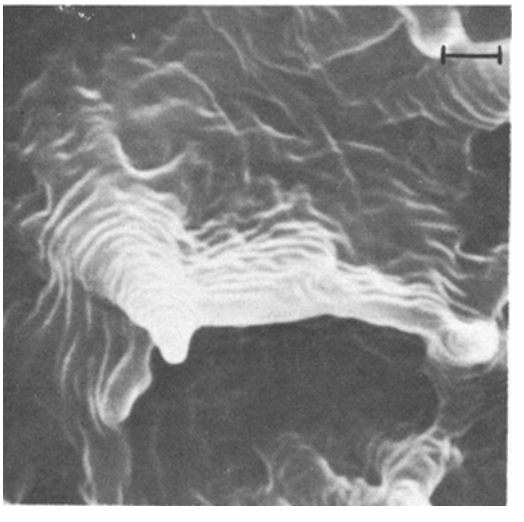

Figure 5 One fibril of Fig. 3 at higher magnification (Scale 1 μm).

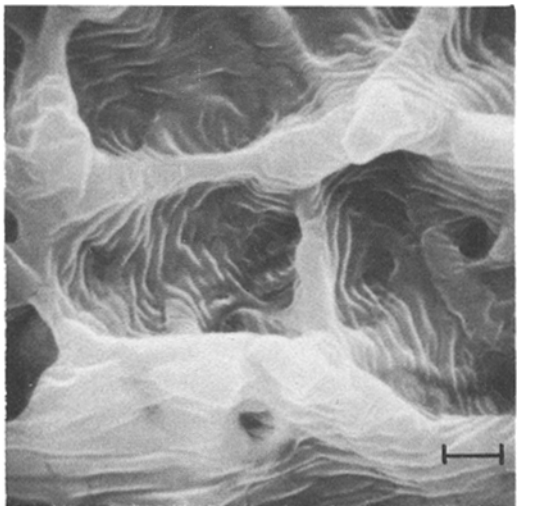

Figure 6 ESC fracture surface, MFI 0.25 (Scale 2 μm).

this point that although the failure appears interlamellar, the individual lamellae have not been resolved; each step probably consists of a stack of lamellae. Figs. 1, 3 and 5 were all taken on an LDPE of MFI 2.5.

Similar interlamellar ESC failures have also been observed for polyethylenes having similar density but different MFI. Fig. 6 shows the ESC fracture surface for a material having MFI of 0.25. A careful observation of the figure shows that, while interlamellar failure is prevalent throughout the fibrils, the final failure, i.e. the physical separation of the tip of the fibril, is also typically cleavage type and interlamellar, suggesting that the onset of the failure and the final failure takes place in the same interlamellar manner. Fig. 7 shows the interlamellar attack in another polyethylene of MFI 20, however, because of the much smoother surface, it is quite difficult to find this type of failure in higher MFI material.

The figures so far have shown the evidence of interlamellar failure in the material somewhat away from the sharp crack tip. The examination of the fracture surface at the boundary of the sharp

Figure 7 ESC fracture surface, MFI 20 (Scale 2 μm).

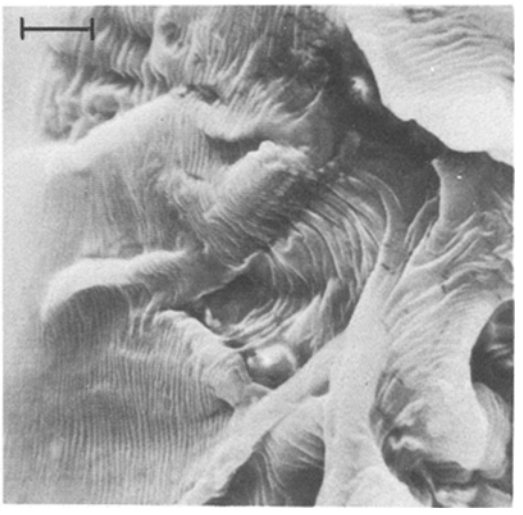

Figure 8 Onset of environmental stress crack propagation from sharp crack tip (extreme left), MFI 0.25 (Scale 5 μm).

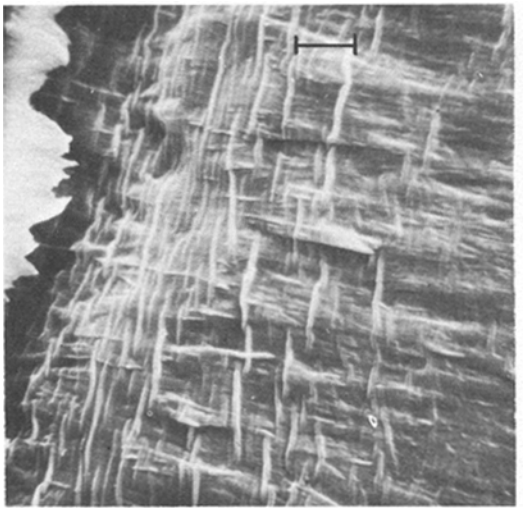

Figure 9 Onset of crack propagation in air from sharp crack tip (extreme left) (Scale 10 μm).

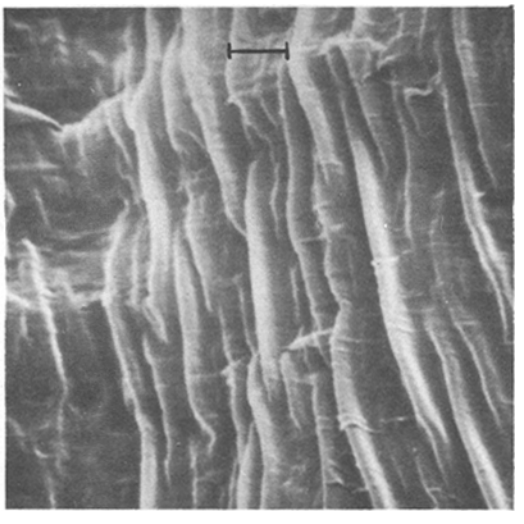

Figure 10 Higher magnification of the striations observed near the crack tip of Fig. 9 (Scale 2 μm).

crack tip and the beginning of crack propagation under load confirms that the ESC failure is interlamellar. Fig. 8 shows that as soon as the load is applied, in the ESC case, the environment starts attacking the interlamellar region.

The micrographs of the material tested in air are quite different. Figs. 9 and 10 show crack-tip boundaries for air-tested materials at two magnifications which show the presence of striations quite unlike those seen in ESC failure. These striations disappear within a very short distance from the sharp crack tip.

These findings show that in low-stress ESC failure the environment attacks the interlamellar regions, and the crack front then finds its way through the interlamellar regions of fibrils which are favourably placed in its path. The final fracture also takes place by the interlamellar failure of the fibril tips without any cold work.

Studies are being undertaken for these and other materials, including high-density polyethylene and the results will be reported later.

Reference

1. M. J. HANNON, *J. Appl. Polymer Sci.* **13** (1974) 3761

Received 18 February
and accepted 11 March 1977.

S. BANDYOPADHYAY,
H. R. BROWN,
Department of Materials Engineering,
Monash University,
Clayton 3168,
Victoria, Australia

Absorption–desorption characteristics of hydrogen for $MmCo_5$

RNi_5 and RCo_5 (R = rare earth metal) absorb and desorb hydrogen reversibly by a pressure operation [1, 2], and are important as hydrogen storage materials. $MmNi_5$, using Mischmetall as R, also readily absorbs and desorbs large amounts of hydrogen, and forms the hydride $MmNi_5H_7$ under 10^6 Pa at room temperature [3]. In this work, the characteristics of $MmCo_5$–H system were studied.

The composition of Mm used was (in wt %); La 32.9, Ce 47.1, Nd 13.9, Pr 4.3, and the other rare earth elements 1.0; the Co was of purity 99.99 wt %. The compounds were prepared by argon-flame melting of the elements in a water-cooled copper crucible and then homogenizing the ingots at 1100° C for 10 h *in vacuo*. After cooling to room temperature, the ingots were crushed to powder of 10 μm average particle diameter. The powders were into a stainless steel specimen holder, and successively heated at 100° C under 0.13 Pa to remove surface contaminants which hinder the absorption of hydrogen before measuring.

The absorption–depsorption characteristics were determined by pressure–composition isotherm measurements. The hydrogen desorption rate from the hydride was obtained by measuring the amount of hydrogen flowing into a measuring cylinder from the specimne holder, and the absorption rate was measured by pressure variation in a measuring system. The reaction between the hydrogen and the compound was examined by high pressure DTA under a hydrogen atmosphere.

The pressure–composition isotherms of $MmCo_5$–H system are shown in Fig. 1. The curves do not show the obvious platau at room temperature, and the absorption and desorption isotherms show hysteresis, which gradually increases with increasing temperature. The dissolved amount of hydrogen in $MmCo_5$ at 25° C and 5×10^4 Pa, determined, from the measurement of the pressure–composition isotherm, was about $MmCo_5H_{0.25}$, and the hydride $MmCo_5H_{2.5}$ was formed at 25° C, 10^6 Pa.

The relationship between the temperature and pressure at the composition $MmCo_5H_{1.25}$ in the absorption and desorption isotherms are shown in Fig. 2. The enthalpy changes for the absorption and desorption of hydrogen calculated from the slopes are −0.34 and 0.25 eV, respectively.

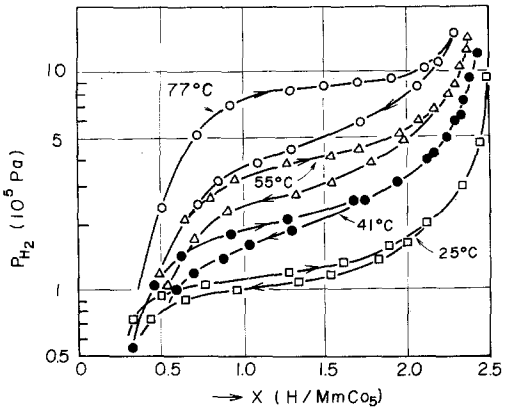

Figure 1 Pressure–composition isotherms for $MmCo_5$–H system.

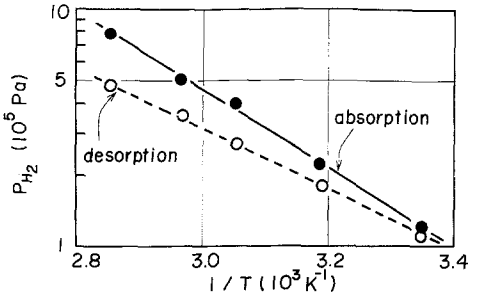

Figure 2 Relationships between the absorption and desorption pressures of hydrogen for $MmCo_5H_{1.25}$ and the reciprocal temperature.